Research Article | Vol. 24, No. 25 | 12 Dec 2016 | OPTICS EXPRESS 28923

Optics EXPRESS

Alignment errors calibration for a channeled spectropolarimeter

BIN YANG,[1,2] XUEPING JU,[1,2] CHANGXIANG YAN,[1] AND JUNQIANG ZHANG[1,*]

[1]*Changchun Institute of Optics, Fine Mechanics and Physics, Chinese Academy of Sciences, Changchun 130033, China*
[2]*University of Chinese Academy of Sciences, Beijing 100049, China*
[*]*zjqciom@sina.com*

Abstract: This paper presents a method to calibrate alignment errors for a channeled spectropolarimeter. A calibration model, including an alignment errors determination model and an alignment errors compensation model, is derived firstly. To determine the exact alignment errors of the high-order retarders and polarizer included in the spectropolarimeter, an auxiliary high-order retarder and a reference beam are used. The auxiliary high-order retarder does not affect the normal use of the spectropolarimeter and the polarization state of the reference beam needs not to be controlled accurately. Based on the determination results, the alignment errors are compensated by using a correction algorithm without any precise mechanical adjustments. Simulation results show that the alignment errors can be determined accurately and the errors of the reconstructed Stokes parameters due to the alignment errors are reduced effectively by the presented method. Finally, experimental results are summarized and analyzed to demonstrate the effectiveness of the calibration method.

OCIS codes: (120.5410) Polarimetry; (120.6200) Spectrometers and spectroscopic instrumentation; (220.1140) Alignment.

References and links

1. S. Jones, F. Iannarilli, and P. Kebabian, "Realization of quantitative-grade fieldable snapshot imaging spectropolarimeter," Opt. Express **12**(26), 6559–6573 (2004).
2. F. Snik, T. Karalidi, and C. U. Keller, "Spectral modulation for full linear polarimetry," Appl. Opt. **48**(7), 1337–1346 (2009).
3. F. Cremer, W. de Jong, and K. Schutte, "Infrared polarization measurements and modeling applied to surface-laid antipersonnel landmines," Opt. Eng. **41**(5), 1021–1032 (2002).
4. N. Hagen, K. Oka, and E. L. Dereniak, "Snapshot Mueller matrix spectropolarimeter," Opt. Lett. **32**(15), 2100–2102 (2007).
5. A. A. Thyparambil, Y. Wei, and R. A. Latour, "Experimental characterization of adsorbed protein orientation, conformation, and bioactivity," Biointerphases **10**(1), 019002 (2015).
6. M. Dubreuil, S. Rivet, B. Le Jeune, and L. Dupont, "Time-resolved switching analysis of a ferroelectric liquid crystal by snapshot Mueller matrix polarimetry," Opt. Lett. **35**(7), 1019–1021 (2010).
7. B. Henderson, "Spectroscopic measurements," in *Handbook of Optics*, M. Bass, ed. (McGraw-Hill, 1995).
8. R. A. Chipman, "Polarimetry," in *Handbook of Optics*, M. Bass, ed. (McGraw-Hill, 1995).
9. J. S. Tyo, D. L. Goldstein, D. B. Chenault, and J. A. Shaw, "Review of passive imaging polarimetry for remote sensing applications," Appl. Opt. **45**(22), 5453–5469 (2006).
10. K. Oka and T. Kato, "Spectroscopic polarimetry with a channeled spectrum," Opt. Lett. **24**(21), 1475–1477 (1999).
11. F. J. Iannarilli, Jr., S. H. Jones, H. E. Scott, and P. Kebabian, "Polarimetric-spectral intensity modulation (P-SIM): Enabling simultaneous hyperspectral and polarimetric imaging," Proc. SPIE **3698**, 474–1477 (1999).
12. K. Oka and T. Kaneko, "Compact complete imaging polarimeter using birefringent wedge prisms," Opt. Express **11**(13), 1510–1519 (2003).
13. R. W. Aumiller, C. Vandervlugt, E. L. Dereniak, R. Sampson, and R. W. McMillan, "Snapshot imaging spectropolarimetry in the visible and infrared," Proc. SPIE **6972**, 69720D (2008).
14. J. Li, J. Zhu, and H. Wu, "Compact static Fourier transform imaging spectropolarimeter based on channeled polarimetry," Opt. Lett. **35**(22), 3784–3786 (2010).
15. J. Craven-Jones, M. W. Kudenov, M. G. Stapelbroek, and E. L. Dereniak, "Infrared hyperspectral imaging polarimeter using birefringent prisms," Appl. Opt. **50**(8), 1170–1185 (2011).
16. T. Mu, C. Zhang, C. Jia, and W. Ren, "Static hyperspectral imaging polarimeter for full linear Stokes parameters," Opt. Express **20**(16), 18194–18201 (2012).

#278748 http://dx.doi.org/10.1364/OE.24.028923
Journal © 2016 Received 14 Oct 2016; revised 30 Nov 2016; accepted 1 Dec 2016; published 6 Dec 2016

Optics EXPRESS

17. T. Mu, C. Zhang, C. Jia, W. Ren, L. Zhang, and Q. Li, "Alignment and retardance errors, and compensation of a channeled spectropolarimeter," Opt. Commun. **294**, 88–95 (2013).
18. M. Locke, D. S. Sabatke, E. L. Dereniak, M. R. Descour, J. P. Garcia, T. Hamilton, and R. W. McMillan, "Snapshot Imaging Spectropolarimeter," Proc. SPIE **4481**, 64–72 (2002).
19. A. Taniguchi, K. Oka, H. Okabe, and M. Hayakawa, "Stabilization of a channeled spectropolarimeter by self-calibration," Opt. Lett. **31**(22), 3279–3281 (2006).

1. Introduction

Spectropolarimetry quantifies the polarization state and spectral content of the light, which plays an important role in many fields, such as remote sensing [1–3], biomedical optics [4,5], and material characterization [6]. Several methods for polarization and spectral measurements have been developed [7–9]. In these methods, Channeled spectropolarimetry, proposed by Oka et al. [10] and Iannarilli et al. [11], is a more attractive approach. It can simultaneously measure the spectra of the four Stokes parameters in a snapshot mode. Furthermore, this method has a simple optical system and uses no mechanically movable components for polarization control. On the basis of this snapshot concept, different types of spectropolarimeters have been presented in recent publications [12–16].

In spite of the advantages, misalignments of the polarimetric spectral intensity modulation (PSIM) module, which is the key component of the channeled spectropolarimeter, have significant influences on the reconstructed Stokes parameters [17]. In addition, the misalignments of the PSIM module, including two high-order retarders and a polarizer, are inevitable in a practical application. Therefore, calibrating the alignment errors is a necessary step when we use the channeled spectropolarimeter. Locke et al. [18] used a 3:1 ratio of retarder thickness to qualitatively check the system alignment, which reduced the available bandwidth at the same time. Mu et al. [17] used two linearly polarized beams oriented at 22.5° and 45° to calibrate the orientation errors of the fast axes of the high-order retarders. However, they ignored the orientation error of the transmission axis of the polarizer used in the spectropolarimeter. To the best of our knowledge, the problem of the misalignments of the channeled spectropolarimeter cannot be well solved with the previous literatures.

To overcome this limitation, the paper presents a method to calibrate the alignment errors for the channeled spectropolarimeter. We use an auxiliary high-order retarder and a reference beam to determine the exact alignment errors. The auxiliary high-order retarder, removed after determining the alignment errors, will not affect the normal use of the channeled spectropolarimeter. For the reference beam, we need not to know its polarization state accurately. We also develop an effective correction algorithm to compensate the alignment errors based on the determination results. By the presented calibration method, the accuracy of the reconstructed Stokes parameters can be improved obviously. In this paper, section 2 provides a brief review of the channeled spectropolarimetry. Section 3 derives a theoretical model for calibrating the alignment errors. In sections 4 and 5, we summary and analyze our simulation and experimental results, respectively. Conclusions are presented in section 6.

2. Principle of the channeled spectropolarimetry

We first briefly review the principle of the channeled spectropolarimetry. The optical schematic of a channeled spectropolarimeter is depicted in Fig. 1. A polychromatic beam passes through the PSIM module, i.e., the high-order retarders, R_1 and R_2 with thicknesses d_1 and d_2, and the polarizer, A, and then is launched into a spectrometer. The fast axes of R_1 and R_2 intersect at an angle of 45°, and the transmission axis of A is aligned with the fast axis of R_1 [10].

Optics EXPRESS

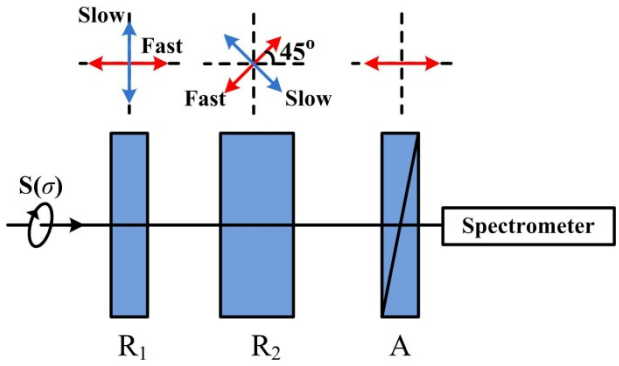

Fig. 1. Schematic of a channeled spectropolarimeter.

The spectrum obtained by the spectrometer is expressed as

$$\begin{aligned} B(\sigma) &= (1/2)S_0(\sigma) + (1/4)\left|S_{23}(\sigma)\right|\cos\{\varphi_2(\sigma) - \varphi_1(\sigma) + \arg[S_{23}(\sigma)]\} \\ &\quad - (1/4)\left|S_{23}(\sigma)\right|\cos\{\varphi_2(\sigma) + \varphi_1(\sigma) - \arg[S_{23}(\sigma)]\} \\ &\quad + (1/2)\left|S_1(\sigma)\right|\cos\{\varphi_2(\sigma) + \arg[S_1(\sigma)]\}, \end{aligned} \tag{1}$$

where $S_{23}(\sigma)=S_2(\sigma)+iS_3(\sigma)$, and $S_k(\sigma),(k=0...3)$ denotes the Stokes parameter of the incident target beam. σ is the wavenumber, arg means the operator to take the argument, and $\varphi_1(\sigma)$ and $\varphi_2(\sigma)$ are the phase retardations of R_1 and R_2, respectively. Computing the autocorrelation function of $B(\sigma)$ by the inverse Fourier transformation, seven channels containing different Stokes components are obtained. If d_1 and d_2 are selected properly, the seven channels are separated from one another over the h domain (where h is variable conjugate to σ under the Fourier transformation). The desired channels can be extracted by using the frequency filtering technique and then performed Fourier transformations to reconstruct the Stokes parameters of the incident target beam. Noteworthy is that this reconstruction procedure is suitable only for a perfectly aligned spectropolarimeter. If the orientations of the fast axes of R_1 and R_2 and the transmission axis of A deviate from their ideal states, the errors of the obtained Stokes parameters will be introduced by using this reconstruction model.

3. Derivation of calibration model

In this section, we derive a model for calibrating the alignment errors of the channeled spectropolarimeter. A two-setup approach is adopted for the alignment errors calibration. The first step involves determining the exact alignment errors, and the second step involves compensating the alignment errors based on the determination results.

3.1 Alignment errors determination

We add an auxiliary high-order retarder in front of the PSIM module to quantify the alignment errors of a channeled spectropolarimeter. The basic configuration for determining the alignment errors is shown in Fig. 2. The high-order retarder R_3, with a thickness d_3, is the auxiliary component in determining the alignment errors. We use the slow axis of R_3 as the x-axis, the fast axis of R_3 as the y-axis and the optical axis as the z-axis to establish a right-handed coordinate system. Theoretically, as described in section 2, the fast axes of R_1 and R_2 are oriented at 0° and 45°, and the transmission axis of A is oriented at 0°, relative to the x-axis, respectively. Realistically, alignment errors of the polarization elements are inevitably introduced, and θ_1, θ_2, and ε indicate the alignment errors of R_1, R_2, and A, respectively.

Optics EXPRESS

To calibrate the alignment errors and measure the state of polarization of light accurately, the thickness ratio of R_1, R_2, and R_3 is designed to be d_1: d_2: d_3 = 1: 2: 0.7.

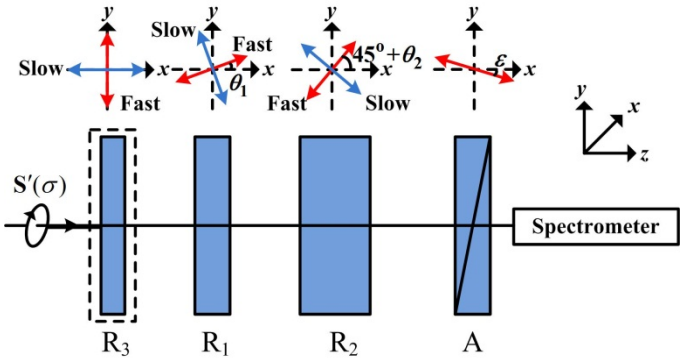

Fig. 2. Schematic of the configuration for determining the alignment errors of a channeled spectropolarimeter. R_3 is marked with a dashed box means that it will be removed after determining the alignment errors.

We firstly compute the Stokes vector of the reference light which passes through R_3 and the PSIM module:

$$\mathbf{S}'_{out}(\sigma)=\mathbf{M}_{\mathrm{A}}(\varepsilon)\cdot\mathbf{M}_{\mathrm{R2}}[45^{\mathrm{o}}+\theta_2,\varphi'_2(\sigma)]\cdot\mathbf{M}_{\mathrm{R1}}[\theta_1,\varphi'_1(\sigma)]\cdot\mathbf{M}_{\mathrm{R3}}[90^{\mathrm{o}},\varphi'_3(\sigma)]\cdot\mathbf{S}'(\sigma), \quad (2)$$

where $\mathbf{M}_{\mathrm{A}}$, $\mathbf{M}_{\mathrm{R2}}$, $\mathbf{M}_{\mathrm{R1}}$, and $\mathbf{M}_{\mathrm{R3}}$ denote the Mueller matrices of A, R_2, R_1, and R_3, respectively, and $\varphi'_2(\sigma)$, $\varphi'_1(\sigma)$, and $\varphi'_3(\sigma)$ are the actual phase retardations of R_2, R_1, and R_3, respectively. The spectrum obtained by the spectrometer is given by

$$\begin{aligned}
B'(\sigma)=&(1/2)S'_0(\sigma)+(1/2)\Gamma_1\left|S'_1(\sigma)\right|\cos\{\varphi'_2(\sigma)+\arg[S'_1(\sigma)]\}\\
&+(1/4)\Gamma_2\left|S'_1(\sigma)\right|\cos\{\varphi'_1(\sigma)+\varphi'_2(\sigma)+\arg[S'_1(\sigma)]\}\\
&-(1/4)\Gamma_2\left|S'_1(\sigma)\right|\cos\{\varphi'_2(\sigma)-\varphi'_1(\sigma)+\arg[S'_1(\sigma)]\}\\
&+(1/4)\Gamma_3\left|S'_{23}(\sigma)\right|\cos\{\varphi'_2(\sigma)-\varphi'_3(\sigma)+\arg[S'_{23}(\sigma)]\}\\
&+(1/4)\Gamma_3\left|S'_{23}(\sigma)\right|\cos\{\varphi'_2(\sigma)+\varphi'_3(\sigma)-\arg[S'_{23}(\sigma)]\}\\
&+(1/4)(\Gamma_4+\Gamma_5-\Gamma_6-\Gamma_7)\left|S'_{23}(\sigma)\right|\cos\{\varphi'_1(\sigma)-\varphi'_3(\sigma)-\arg[S'_{23}(\sigma)]\}\\
&+(1/8)(\Gamma_8-\Gamma_9+\Gamma_{10}+\Gamma_6-\Gamma_3+\Gamma_7)\left|S'_{23}(\sigma)\right|\cos\{\varphi'_2(\sigma)+\varphi'_3(\sigma)-\varphi'_1(\sigma)+\arg[S'_{23}(\sigma)]\}\\
&-(1/8)(\Gamma_8+\Gamma_9+\Gamma_{10}-\Gamma_6+\Gamma_3-\Gamma_7)\left|S'_{23}(v)\right|\cos\{\varphi'_1(\sigma)+\varphi'_2(\sigma)-\varphi'_3(\sigma)-\arg[S'_{23}(\sigma)]\},
\end{aligned} \quad (3)$$

where $S'_{23}(\sigma)$=$S'_2(\sigma)$+$iS'_3(\sigma)$, and $S'_k(\sigma)$, $(k=0...3)$ denotes the Stokes parameter of the incident reference beam. $\varphi'_j(\sigma)=2\pi\sigma d_j\Delta n(\sigma)+\Delta\varphi_j(\sigma),(j=1,2,3)$, where $\Delta n(\sigma)$ is the birefringence of the crystal. $\Delta\varphi_j(\sigma)$ denotes the additional phase retardation of R_j due to external factors, and $\Gamma_n,(n=1...10)$ can be expressed as

$$\begin{cases}\Gamma_1=b^2d^2f & \Gamma_2=adf & \Gamma_3=abd^2f & \Gamma_4=bd^2\mathrm{e} & \Gamma_5=b^2d^2\mathrm{e}\\ \Gamma_6=bcdf & \Gamma_7=b^2cdf & \Gamma_8=df & \Gamma_9=ad^2f & \Gamma_{10}=bdf\end{cases}, \quad (4)$$

where $a=\sin(2\theta_1)$, $b=\cos(2\theta_1)$, $c=\sin(2\theta_2)$, $d=\cos(2\theta_2)$, $e=\sin(2\varepsilon)$, and $f=\cos(2\varepsilon)$. Because the alignment errors are typically small, a, c, and e can be regarded as small quantities. Hence, when we deduce the expression for $B'(\sigma)$, we ignore the second order small quantities such as a^2, c^2, e^2, ac, ae, and ce.

Optics EXPRESS

We can obtain the autocorrelation function of $B'(\sigma)$ by using the inverse Fourier transformation:

$$\begin{aligned} C(h) = {} & C_0(h) + C_1[h-(L_1-L_3)] + C_1^*[-h-(L_1-L_3)] \\ & + C_2[h-(L_2-L_1)] + C_2^*[-h-(L_2-L_1)] \\ & + C_3[h-(L_2-L_3)] + C_3^*[-h-(L_2-L_3)] \\ & + C_4[h-(L_2+L_3-L_1)] + C_4^*[-h-(L_2+L_3-L_1)] \\ & + C_5(h-L_2) + C_5^*(-h-L_2) \\ & + C_6[h-(L_1+L_2-L_3)] + C_6^*[-h-(L_1+L_2-L_3)] \\ & + C_7[h-(L_2+L_3)] + C_7^*[-h-(L_2+L_3)] \\ & + C_8[h-(L_1+L_2)] + C_8^*[-h-(L_1+L_2)], \end{aligned} \tag{5}$$

where

$$C_0 = \mathcal{F}^{-1}[(1/2)S_0(\sigma)], \tag{6}$$

$$C_1 = \mathcal{F}^{-1}\{(1/8)(\Gamma_4+\Gamma_5-\Gamma_6-\Gamma_7)S_{23}^*(\sigma)\exp\{i[\varphi_1'(\sigma)-\varphi_3'(\sigma)]\}\}, \tag{7}$$

$$C_2 = \mathcal{F}^{-1}\{(-1/8)\Gamma_2 S_1(\sigma)\exp\{i[\varphi_2'(\sigma)-\varphi_1'(\sigma)]\}\}, \tag{8}$$

$$C_3 = \mathcal{F}^{-1}\{(1/8)\Gamma_3 S_{23}(\sigma)\exp\{i[\varphi_2'(\sigma)-\varphi_3'(\sigma)]\}\}, \tag{9}$$

$$C_4 = \mathcal{F}^{-1}\{(1/16)(\Gamma_8-\Gamma_9+\Gamma_{10}+\Gamma_6-\Gamma_3+\Gamma_7)S_{23}(\sigma)\exp\{i[\varphi_2'(\sigma)+\varphi_3'(\sigma)-\varphi_1'(\sigma)]\}\}, \tag{10}$$

$$C_5 = \mathcal{F}^{-1}\{(1/4)\Gamma_1 S_1(\sigma)\exp\{i[\varphi_2'(\sigma)]\}\}, \tag{11}$$

$$C_6 = \mathcal{F}^{-1}\{(-1/16)(\Gamma_8+\Gamma_9+\Gamma_{10}-\Gamma_6+\Gamma_3-\Gamma_7)S_{23}^*(\sigma)\exp\{i[\varphi_1'(\sigma)+\varphi_2'(\sigma)-\varphi_3'(\sigma)]\}\}, \tag{12}$$

$$C_7 = \mathcal{F}^{-1}\{(1/8)\Gamma_3 S_{23}^*(\sigma)\exp\{i[\varphi_2'(\sigma)+\varphi_3'(\sigma)]\}\}, \tag{13}$$

$$C_8 = \mathcal{F}^{-1}\{(1/8)\Gamma_2 S_1(\sigma)\exp\{i[\varphi_1'(\sigma)+\varphi_2'(\sigma)]\}\}, \tag{14}$$

and L_j is the actual optical path difference (OPD) introduced by R_j in the central wavenumber [14]. The seventeen channels are separated from one another over the h axis if d_1, d_2, and d_3 are selected properly. The desired channels, C_1, C_3, C_4, C_5, C_6, C_7, and C_8, centered at $h = L_1 - L_3$, $L_2 - L_3$, $L_2 + L_3 - L_1$, L_2, $L_1 + L_2 - L_3$, $L_2 + L_3$, and $L_1 + L_2$, respectively, are then filtered out by the frequency filtering technique and performed Fourier transformations independently. We assume that $\theta_1 > 0$, $\theta_2 > 0$, and $\varepsilon < 0$, which indicate that the fast axes of R_1 and R_2 deviate from their ideal states in a counterclockwise direction while the transmission axis of A deviates from its ideal state in a clockwise direction. We should mention that these conditions are dependent on the manufacturing tolerances of the channeled spectropolarimeter. Then, we can determine the sign of the coefficient of each term in Eq. (5), such as $(\Gamma_4+\Gamma_5-\Gamma_6-\Gamma_7) < 0$, $\Gamma_2 > 0$, $\Gamma_3 > 0$, $(\Gamma_8-\Gamma_9+\Gamma_{10}+\Gamma_6-\Gamma_3+\Gamma_7) > 0$, $\Gamma_1 > 0$, and $(\Gamma_8+\Gamma_9+\Gamma_{10}-\Gamma_6+\Gamma_3-\Gamma_7) > 0$. To avoid the inconvenience that any term in Eq. (5) may be zero, we should choose the reference beam with $S_1 \neq 0$ and $S_2 \neq 0$ or $S_3 \neq 0$, however, we need not to know its polarization state accurately.

Using the Fourier transformations of the channels C_1, C_3, C_4, C_5, C_6, C_7, and C_8, we can calculate out that

Optics EXPRESS

$$abs[\frac{\mathcal{F}(C_8)}{\mathcal{F}(C_5)}]=\frac{a}{2b^2d}, \tag{15}$$

$$abs[\frac{\mathcal{F}(C_4)}{\mathcal{F}(C_3)}]+abs[\frac{\mathcal{F}(C_6)}{\mathcal{F}(C_7)}]=\frac{b+1}{abd}, \tag{16}$$

$$abs[\frac{\mathcal{F}(C_6)}{\mathcal{F}(C_7)}]-abs[\frac{\mathcal{F}(C_4)}{\mathcal{F}(C_3)}]=\frac{(ad-bc)(b+1)}{abd}, \tag{17}$$

$$abs[\frac{\mathcal{F}(C_1)}{\mathcal{F}(C_7)}]=\frac{bd(b+1)(cf-de)}{abd^2f}, \tag{18}$$

where *abs* stands for the operation of taking the absolute value. Meanwhile, *a*, *b*, *c*, *d*, *e*, and *f* satisfy the following equations: $a^2+b^2=1$, $c^2+d^2=1$, and $e^2+f^2=1$. Substituting these equations into Eqs. (15)–(18) yields the determination results of *b*, *c*, and *e*, i.e.,

$$b=\frac{Q}{Q+2N}, \tag{19}$$

$$c=-\frac{Wb}{Q}+\sqrt{(\frac{Wb}{Q})^2-(\frac{W}{Q})^2-b^2+1}, \tag{20}$$

$$e=-\sqrt{\frac{(Qbc-H)^2}{Q^2b^2(1-c^2)+(Qbc-H)^2}}, \tag{21}$$

where

$$\begin{cases} Q=abs[\frac{\mathcal{F}(C_4)}{\mathcal{F}(C_3)}]+abs[\frac{\mathcal{F}(C_6)}{\mathcal{F}(C_7)}] & N=abs[\frac{\mathcal{F}(C_8)}{\mathcal{F}(C_5)}] \\ W=abs[\frac{\mathcal{F}(C_6)}{\mathcal{F}(C_7)}]-abs[\frac{\mathcal{F}(C_4)}{\mathcal{F}(C_3)}] & H=abs[\frac{\mathcal{F}(C_1)}{\mathcal{F}(C_7)}] \end{cases}. \tag{22}$$

The alignment errors, θ_1, θ_2, and ε, are given by $\theta_1=(1/2)\arccos(b)$, $\theta_2=(1/2)\arcsin(c)$, and $\varepsilon=(1/2)\arcsin(e)$, respectively.

3.2 Alignment errors compensation

Based on the determination results, we can adjust the states of the polarization elements with precise mechanical devices. However, if an algorithm for correction, which can compensate the alignment errors, is developed, the mechanical adjustments will no longer be required. In the following, an effective correction algorithm will be presented.

When R_3 is removed after determining the alignment errors, the Mueller matrix of the target light launched into the spectrometer is

$$\mathbf{S}_{out}(\sigma)=\mathbf{M}_{\mathrm{A}}(\varepsilon)\cdot\mathbf{M}_{\mathrm{R}2}[45^{\circ}+\theta_2,\varphi_2'(\sigma)]\cdot\mathbf{M}_{\mathrm{R}1}[\theta_1,\varphi_1'(\sigma)]\cdot\mathbf{S}(\sigma). \tag{23}$$

The spectrum measured by the spectrometer becomes

Optics EXPRESS

$$
\begin{aligned}
B(\sigma) &= (1/2)S_0(\sigma) + (1/2)bd^2 f(bS_1(\sigma) + aS_2(\sigma))\cos[\varphi_2'(\sigma)] \\
&\quad -(1/8)(\Gamma_8 + \Gamma_6 - \Gamma_9)[aS_1(\sigma) - bS_2(\sigma) - iS_3(\sigma)]\exp\{i[\varphi_2'(\sigma) - \varphi_1'(\sigma)]\} \\
&\quad -(1/8)(\Gamma_8 + \Gamma_6 - \Gamma_9)[aS_1(\sigma) - bS_2(\sigma) + iS_3(\sigma)]\exp\{-i[\varphi_2'(\sigma) - \varphi_1'(\sigma)]\} \\
&\quad +(1/4)(\Gamma_6 - \Gamma_4)[-bS_2(\sigma) + iS_3(\sigma)]\exp[i\varphi_1(\sigma)] \\
&\quad +(1/4)(\Gamma_6 - \Gamma_4)[-bS_2(\sigma) - iS_3(\sigma)]\exp[-i\varphi_1(\sigma)] \\
&\quad +(1/8)(\Gamma_8 - \Gamma_6 + \Gamma_9)[aS_1(\sigma) - bS_2(\sigma) + iS_3(\sigma)]\exp\{i[\varphi_2'(\sigma) + \varphi_1'(\sigma)]\} \\
&\quad +(1/8)(\Gamma_8 - \Gamma_6 + \Gamma_9)[aS_1(\sigma) - bS_2(\sigma) - iS_3(\sigma)]\exp\{-i[\varphi_2'(\sigma) + \varphi_1'(\sigma)]\}.
\end{aligned} \tag{24}
$$

When we deduce the expression for $B(\sigma)$, we also ignore the terms containing the second order small quantities. The inverse Fourier transformation of $B(\sigma)$ gives the autocorrelation:

$$
\begin{aligned}
A(h) &= A_0(h) + A_1(h - L_1) + A_1^*(-h - L_1) \\
&\quad + A_2[h - (L_2 - L_1)] + A_2^*[-h - (L_2 - L_1)] \\
&\quad + A_3(h - L_2) + A_3^*(-h - L_2) \\
&\quad + A_4[h - (L_2 + L_1)] + A_4^*[-h - (L_2 + L_1)],
\end{aligned} \tag{25}
$$

where

$$A_0 = \mathcal{F}^{-1}[(1/2)S_0'(\sigma)], \tag{26}$$

$$A_1 = \mathcal{F}^{-1}\{(1/4)(\Gamma_6 - \Gamma_4)[-bS_2'(\sigma) + iS_3'(\sigma)]\exp[i\varphi_1'(\sigma)]\}, \tag{27}$$

$$A_2 = \mathcal{F}^{-1}\{-(1/8)(\Gamma_8 + \Gamma_6 - \Gamma_9)[aS_1'(\sigma) - bS_2'(\sigma) - iS_3'(\sigma)]\exp\{i[\varphi_2'(\sigma) - \varphi_1'(\sigma)]\}\}, \tag{28}$$

$$A_3 = \mathcal{F}^{-1}\{(1/4)\Gamma_{10}d[bS_1'(\sigma) + aS_2'(\sigma)]\exp[i\varphi_2'(\sigma)]\}, \tag{29}$$

$$A_4 = \mathcal{F}^{-1}\{(1/8)(\Gamma_8 - \Gamma_6 + \Gamma_9)[aS_1'(\sigma) - bS_2'(\sigma) + iS_3'(\sigma)]\exp\{i[\varphi_2'(\sigma) + \varphi_1'(\sigma)]\}\}, \tag{30}$$

We can find that there are nine channels included in $A(h)$. Compared with the autocorrelation function of the obtained spectrum given in [10], the autocorrelation function here becomes more complicated due to the alignment errors of R_1, R_2, and A. Especially, two additional channels, centered at $\pm L_1$, are introduced. Considering the thickness ratio of R_1 and R_2 is d_1: d_2 = 1: 2, the phase retardation $\varphi_1'(\sigma)$ is approximately equal to the phase retardation $[\varphi_2'(\sigma) - \varphi_1'(\sigma)]$. As a result, the channels A_1 and A_2 are hardly separated from each other over the h axis. To avoid channel aliasing, we choose the channels A_0, A_3, and A_4, centered at $h = 0$, L_2, and $L_1 + L_2$, respectively, to reconstruct the Stokes parameters of the target light. By filtering out the desired channels and performing Fourier transformations independently, we can obtain the results:

$$\mathcal{F}(A_1) = (1/2)S_0(\sigma), \tag{31}$$

$$\mathcal{F}(A_3) = (1/4)d\Gamma_{10}[bS_1(\sigma) + aS_2(\sigma)]\exp[i\varphi_2'(\sigma)], \tag{32}$$

$$\mathcal{F}(A_4) = (1/8)(\Gamma_8 - \Gamma_6 + \Gamma_9)[aS_1(\sigma) - bS_2(\sigma) + iS_3(\sigma)]\exp\{i[\varphi_2'(\sigma) + \varphi_1'(\sigma)]\}, \tag{33}$$

Combining Eqs. (31)–(33) and simplifying yields the reconstructed Stokes parameters of the target light as follows: $S_0(\sigma) = 2\mathcal{F}(A_1)$, $S_1(\sigma) = aE_2(\sigma) + bE_1(\sigma)$, $S_2(\sigma) = aE_1(\sigma) - bE_2(\sigma)$, and $S_3(\sigma) = E_3(\sigma)$. The variables, $E_1(\sigma)$, $E_2(\sigma)$, and $E_3(\sigma)$, are given by

Optics EXPRESS

$$E_1(\sigma)=\frac{4\mathcal{F}(A_3)}{d\Gamma_{10}\exp[i\varphi_2'(\sigma)]}, \tag{34}$$

$$E_2(\sigma)=\frac{8\,\mathrm{Re}\{\mathcal{F}(A_4)/\exp\{i[\varphi_2'(\sigma)+\varphi_1'(\sigma)]\}\}}{\Gamma_8-\Gamma_6+\Gamma_9}, \tag{35}$$

$$E_3(\sigma)=\frac{8\,\mathrm{Im}\{\mathcal{F}(A_4)/\exp\{i[\varphi_2'(\sigma)+\varphi_1'(\sigma)]\}\}}{\Gamma_8-\Gamma_6+\Gamma_9}, \tag{36}$$

where $\exp[i\varphi_2'(\sigma)]$ and $\exp\{i[\varphi_2'(\sigma)+\varphi_1'(\sigma)]\}$ are measured with the method named "reference beam calibration technique" [15,19]. Using a 22.5° linearly polarized beam, the phase terms can be given by

$$\exp[i\varphi_2'(\sigma)]=\frac{2\sqrt{2}}{(\Gamma_1+\Gamma_3)}\cdot\frac{\mathcal{F}(A_{3,22.5^\circ})}{\mathcal{F}(A_{0,22.5^\circ})}, \tag{37}$$

$$\exp\{i[\varphi_1'(\sigma)+\varphi_2'(\sigma)]\}=\frac{4\sqrt{2}}{(a-b)(\Gamma_8-\Gamma_6+\Gamma_9)}\cdot\frac{\mathcal{F}(A_{4,22.5^\circ})}{\mathcal{F}(A_{0,22.5^\circ})}. \tag{38}$$

Since the alignment errors are considered in the presented demodulation model, the reconstructed Stokes parameters based on it will be more accurate. Though the form of the derived model becomes more complex, the added parts contain only the simple trigonometric functions and four-arithmetic operations, which will not lead to difficulties in the reconstruction of the Stokes parameters.

4. Simulation analysis

The effectiveness and advantages of the presented method are firstly validated by simulations. In the simulations, we use a 22.5° linearly polarized beam as the reference light to determine the alignment errors and phase terms, and the wavenumber range is 11111cm^{-1}–16667cm^{-1}. The thicknesses of R_1, R_2, and R_3 are 3.5mm, 7mm, and 2.45mm, respectively. The retarders are made of quartz, whose birefringence in the selected waveband can be found in [8]. The input alignment errors of R_1, R_2, and A are θ_1=0.5°, θ_2=0.5°, and $\varepsilon=-0.5^\circ$, respectively.

Figure 3 shows the magnitude of the autocorrelation function $C(h)$. The seventeen channels are separated from one another over the h axis, which indicates that the thicknesses of the retarders are selected properly. The channels C_1, C_2, C_3, C_4, C_5, C_6, C_7, and C_8 are centered at 10.0μm, 33.6μm, 43.7μm, 57.4μm, 67.4μm, 77.3μm, 90.6μm, and 100.7μm, respectively, which is consistent with the theoretical model calculation.

The alignment errors can then be calculated, which are shown in Fig. 4. Because the alignment errors are independent of wavenumber, we can use the averages of the calculated values in different wavenumbers as the final determination results. Table 1 shows the averages and errors of the determination results of θ_1, θ_2, and ε. These results indicate that we can determine the alignment errors accurately using the presented method, which lays the foundation for compensating the errors in the next step. Furthermore, When determining the alignment errors, we do not use the polarization state of the reference light and just need to assure that the reference light provides $S_1\neq 0$ and $S_2\neq 0$ or $S_3\neq 0$. Compared with the method presented by Mu et al. [17], which uses two linearly polarized beams oriented at 22.5° and 45° to determine the alignment errors of the retarders, we can eliminate several error sources and improve the efficiency in the progress of calibration. To validate the analysis, we also determine the alignment errors with the reference light including the error of angle of

Optics EXPRESS

polarization (AOP) in our simulations, and conclude that the input polarization state does not influence the determination results of the alignment errors.

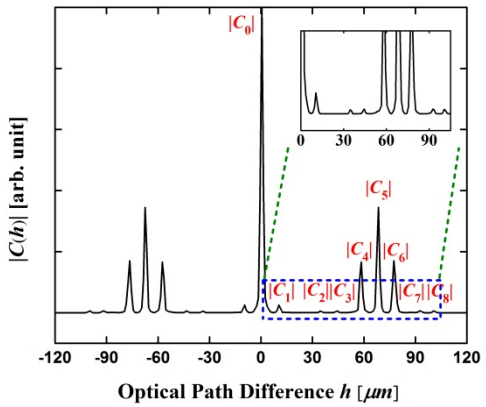

Fig. 3. Magnitude of the autocorrelation function of the obtained spectrum when determining the alignment errors. The part in the dashed box is enlarged.

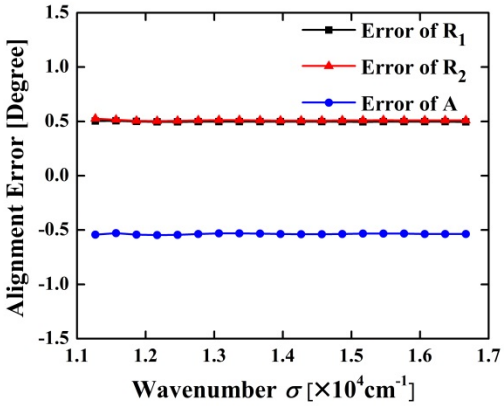

Fig. 4. Determination results of the alignment errors of R_1, R_2, and A.

Table 1. Averages and Errors of the Determination Results of θ_1, θ_2, and ε

Parameter	Input value (°)	Calculated value (°)	Error (°)
θ_1	0.5	0.497	–0.003
θ_2	0.5	0.511	0.011
ε	–0.5	–0.538	–0.038

The magnitude of the autocorrelation function $A(h)$ is depicted in Fig. 5. We can find that the channels A_0, A_3, and A_4 are separated from one another, and the channels A_1 and A_2, both centered at about 33.6μm, are mixed together. These results demonstrate that we cannot use the channels A_1 and A_2 to reconstruct the Stokes parameters. Figure 6 shows the reconstructed Stokes parameters under the input alignment errors. We use two methods to demodulate the Stokes parameters, i.e., a traditional method [15,19] and the new method presented here. With the traditional method, which neglects the misalignments of the PSIM module, the maximum

Optics EXPRESS

deviations of S_1/S_0, S_2/S_0, and S_3/S_0 are 6.44 × 10^{-3}, 6.87 × 10^{-3}, and 2.60 × 10^{-4}, respectively. Analysis suggests that the errors of the reconstructed Stokes parameters are mainly introduced by the alignment errors. By using the presented correction algorithm, the maximum deviations of S_1/S_0, S_2/S_0, and S_3/S_0 are reduced to 1.23 × 10^{-4}, 3.49 × 10^{-4}, and 8.62 × 10^{-5}, respectively. The errors of the reconstructed Stokes parameters are reduced by one order of magnitude compared with the results obtained by the traditional method. That is to say, the errors of the reconstructed results due to the misalignments can be compensated effectively.

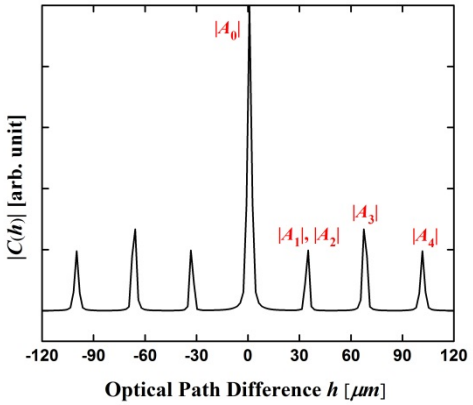

Fig. 5. Magnitude of the autocorrelation function of the obtained spectrum when measuring the target light.

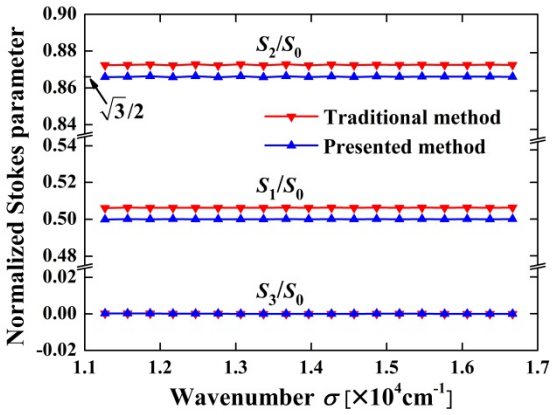

Fig. 6. Reconstructed normalized Stokes parameters. Theoretical values are $S_1/S_0 = 1/2$, $S_2/S_0 = \sqrt{3}/2$, and $S_3/S_0 = 0$.

The above results suggest that the alignment errors of R_1, R_2, and A can be determined accurately and compensated effectively without any precise mechanical adjustments. The presented method can work well under the misalignment of 0.5°, which indicates that this method achieves a high accuracy in the calibration of the alignment errors. In addition, the calibration method needs not to accurately control the polarization state of the reference light to determine the alignment errors. Therefore, the accuracy and efficiency of the calibration procedure are improved.

Optics EXPRESS

5. Experimental results

The experimental configuration for alignment errors calibration can be seen in Fig. 7, where the channeled spectropolarimeter consists of the PSIM module and a spectrometer (FieldSpec 3, Analytical Spectral Devices). The thicknesses of R_1, R_2, and R_3, the reference beam, the target beam, and the wavenumber range are consistent with the simulation settings. A stabilized tungsten halogen lamp, a collimator, and a rotatable polarizer, P, are used to generate the reference and target beams.

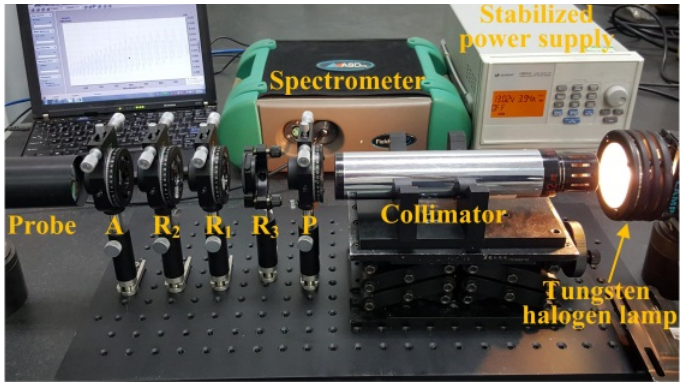

Fig. 7. Photograph of the experimental configuration. The polarizers, P and A, and the high-order retarders, R_1, R_2, and R_3, are installed in precision adjusting racks.

When conducting the experiments of determining the alignment errors, we change the alignment errors of R_1 and R_2, θ_1 and θ_2, from 0.3° to 1.5°, and the alignment error of A, ε, from –0.3° to –1.5°, respectively. Meanwhile, the states of other experimental devices remain unchanged. We provide the measured result at $\theta_1=\theta_2=0.3^\circ$ and $\varepsilon=-0.3^\circ$, shown in Fig. 8. We find that the measured spectrum is modulated with the phase retardations of the three high-order retarders. The inverse Fourier transformation gives the autocorrelation function of the measured spectrum, i.e., the OPD spectrum. In Fig. 8(b), the desired channels are separated from one another and their distributions are consistent with the simulation results, which further validate the presented alignment errors determination model. However, noteworthy is that the channels shift positions slightly over the h axis compared with the simulation results, which may be caused by the thickness errors of the high-order retarders, noise, stray light, and other environmental factors. Based on the alignment errors determination model described in subsection 3.1, we can calculate the alignment errors from the measurements.

The target light is measured after determining the alignment errors. Figure 9 gives the Stokes parameters reconstructed from measurements under different alignment errors. If the reconstructed Stokes parameters are insensitive to the alignment errors, the reconstructed results for the stabilized target light will be constant. However, the errors of the reconstructed Stokes parameters obtained using the traditional method, shown in Fig. 9(a), grow larger as the alignment errors increase. Therefore, to improve demodulation accuracy, the alignment errors of the polarization elements cannot be ignored. In Fig. 9(b), the alignment errors are determined and compensated with the correction algorithm. It is clear that the reconstructed Stokes parameters under different alignment errors are almost overlap each other by using the presented calibration method. The residual errors of S_1/S_0, S_2/S_0, and S_3/S_0 are less than 3.0×10^{-3}, 7.0×10^{-3}, and 2.0×10^{-3}, respectively. The results indicate that the reconstructed Stokes parameters using the presented method, are almost unaffected by the alignment errors, which also means that the manufacturing tolerances of the polarization elements used in the channeled spectropolarimeter are loosened.

Optics EXPRESS

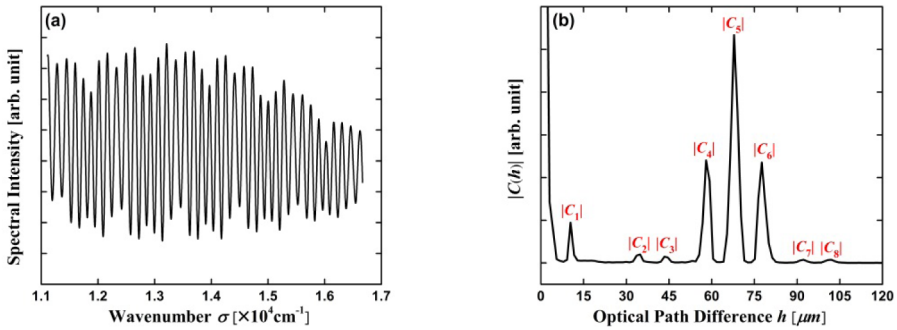

Fig. 8. Measured result in the progress of determining the alignment errors. (a) measured spectral intensity; (b) magnitude of the desired part of the measured spectrum's autocorrelation function.

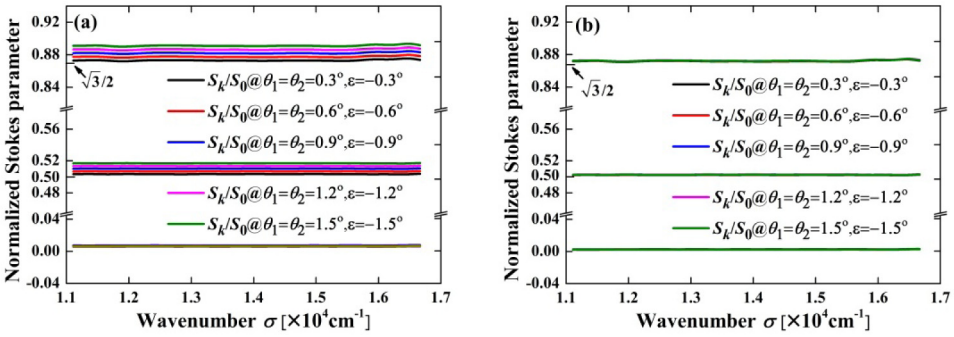

Fig. 9. Stokes parameters reconstructed from experimental measurements under variations of the alignment errors using (a) the traditional method and (b) the presented method. Theoretical reference values are $S_1 / S_0 = 1/2$, $S_2 / S_0 = \sqrt{3}/2$, and $S_3 / S_0 = 0$.

The experimental results show that by using the presented calibration method, the accuracy of the reconstructed Stokes parameters under alignment errors can be improved. In addition to the alignment errors due to machining and assembly, the states of the polarization elements may be changed by vibration, stress, or other factors in an application. To maintain the accuracy of the Stokes parameters reconstructed from the measurement, we can use the presented method to calibrate the channeled spectropolarimeter termly, which has an important significance for the application of the channeled spectropolarimeter.

6. Conclusion

In this paper, we present a method to calibrate the alignment errors for a channeled spectropolarimeter. The calibration will not lead to difficulties in the reconstruction of the Stokes parameters, though the form of the derived calibration model, including the alignment errors determination model and alignment errors compensation model, looks like complex. We can determine the alignment errors of the high-order retarders and polarizer used in the spectropolarimeter with an auxiliary high-order retarder and a reference beam. The reference beam just requires to provide that $S_1 \neq 0$ and $S_2 \neq 0$ or $S_3 \neq 0$, and therefore the error of the AOP of the reference light does not influence the determination results of the alignment errors. Based on the determination results, we can compensate the alignment errors by using a correction algorithm without any precise mechanical adjustments. Simulation and experimental results suggest that the alignment errors of the high-order retarders and polarizer

Optics EXPRESS

can be determined accurately and compensated effectively using the presented calibration method. In this way, the accuracy of the reconstructed Stokes parameters is not affected by the alignment errors and the manufacturing tolerances of the channeled spectropolarimeter are loosened. Given these advantages, the presented method can be used to perform a fast and accurate calibration for the channeled spectropolarimeter termly to improve the accuracy of the reconstructed Stokes parameters.

Funding

National Natural Science Foundation of China (NSFC) (61505199); Program 863 (2011AA12A103).

Acknowledgments

The authors would like to thank Dong Wang for his help in the derivation of the calibration model.